Insight into structural, elastic, phonon, and thermodynamic properties of α-sulfur and energy-related sulfides: A comprehensive first-principles study†

ShunLi Shang,*[a] Yi Wang,[a] Pinwen Guan,[a] William Y. Wang,[a] Huazhi Fang,[a] Tim Anderson,[b] and Zi-Kui Liu[a]

[a]*Department of Materials Science and Engineering, The Pennsylvania State University, University Park, Pennsylvania 16802, USA.*

[b]*Department of Chemical Engineering, University of Florida, Gainesville, Florida 32611, USA*

†: Electronic supplementary information (ESI) available. *E-mail: sus26@psu.edu*

===================================

Table of contents entry

Color graphic
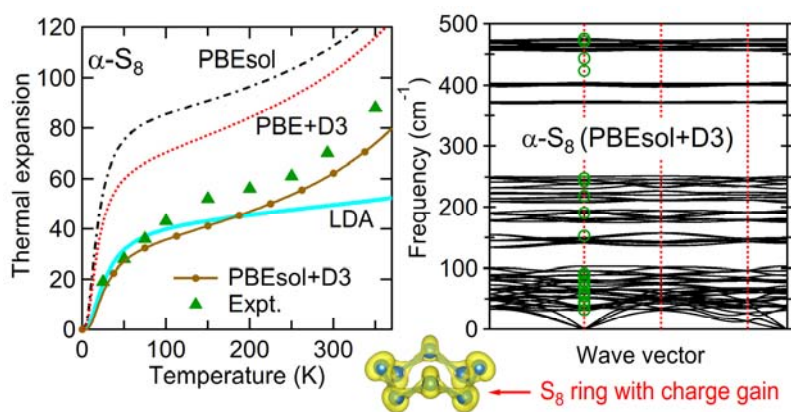
One sentence summary

Current advance of first-principles methodology, comprehensive properties, quantitative bonding and non-polar nature were revealed for α-sulfur and validated by sulfides.

Abstract:

Earth-abundant and nontoxic sulfur (S) is emerging as a key element for developing new materials for sustainable energy. Knowledge gaps, however, still remain regarding the fundamental properties of sulfur especially on a theoretical level. Here, a comprehensive first-principles study has been performed to examine the predicted structural, elastic, phonon, thermodynamic, and optical properties of α-S_8 (α-S) as well as energy-related sulfides. A variety of exchange-correction (X-C) functionals and van der Waals correction in terms of the D3 method have been tested to probe the capability of first-principles calculations. Comparison of predicted quantities with available experimental data indicates that (i) the structural information of α-S are described very well using an improved generalized gradient approximation of PBEsol; (ii) the band gap and dielectric tensor of α-S are calculated perfectly using a hybrid X-C functional of HSE06; (iii) the phonon and elastic properties of α-S are predicted reasonably well using for example the X-C functionals of LDA and PBEsol, and in particular the PBE+D3 and the PBEsol+D3 method; and (iv) the thermodynamic properties of α-S are computed accurately using the PBEsol+D3 method. Examinations using Li_2S, CuS, ZnS, Cu_2ZnSnS_4 (CZTS), SnS, Sn_2S_3, SnS_2, β-S_8 (β-S), and γ-S_8 (γ-S) validate further the crucial role of the van der Waals correction, and thus suggesting the X-C functionals being PBEsol+D3 and PBE+D3 (and PBEsol in some cases) for sulfur as well as S-containing materials. We also examine the possibility by using the Debye model to predict thermodynamic properties of unusual materials, for example, α-S. In addition, the bonding characteristic and non-polar nature of α-S have been revealed quantitatively from phonon calculations and qualitatively from the differential charge density.

1. Introduction

Sustainably satisfying the world's future energy needs, which are estimated at 30 terawatt of new power by 2050,[1] will require development of new materials for energy conversion and storage. This vision includes the need for use of earth-abundant and nontoxic elements such as sulfur (S). This element is particularly challenging as it is the one with the largest number of solid allotropes (around 30 reported).[2-3] The most thermodynamically stable allotrope under standard temperature and pressure (STP) is an orthorhombic cyclo-octasulfur with space group *Fddd*,[2-3] i.e., α-S_8 (labeled as α-S for simplicity in the present work and its structure is given in Figure 1). In addition, the other two crystalline phases consisting of S_8 rings are β-S_8 (β-S) and γ-S_8 (γ-S), as detailed in Table 1. A significant number of metal-based (including Ag, Bi, Co, Cu, Fe, Ge, In, Mn, Mo, Ni, Sb, Sn, V, W, and Zn) sulfides/chalcogenides have been developed for energy conversion and storage applications that include fuel cells, photoelectrochemical water splitting cells, solar cells, Li-ion batteries, and supercapacitors.[4-5] Current examples of earth-abundant photovoltaic absorbers include $Cu_2ZnSn(S,Se)_4$,[6-7] $CuSbS_2$,[8] Fe_2GeS_4,[9] SnS,[6] SnS_2,[6] ZnS,[6, 10] and Cu_2S.[6] As another example, the Li-S battery is notable for its high energy density,[11-12] and multiple S-containing solid electrolytes have been developed for all-solid-state batteries (e.g., $Li_{10}GeP_2S_{12}$,[13] Li_4SnS_4,[14] Li_3PS_4,[15-16] $Li_7P_3S_{11}$,[17] Li_3AsS_4,[18] and Li_2S-P_2S_5[19-20]). In addition, α-S crystals are used as a visible-light-active photocatalyst;[21] CoS_2 has the potential as an earth-abundant electrocatalyst for hydrogen evolution reaction;[22] and MoS_2 can be used for energy conversion and piezotronics,[23] catalytic hydrogen generation,[24] and photodetectors.[25]

Despite the major role of sulfur in emerging energy materials and considerable effort on using first-principles calculations preformed to predict the characteristics of sulfur (e.g., α-S)[21, 26] and

sulfides,[16-17, 27-33] the fundamental physical and chemical properties related to structure, phonon, elasticity, and thermodynamics are still lacking in the literature for sulfur and even for α-S. As example, the needed enthalpy of formation[27, 29, 34] and temperature-pressure-composition growth windows for syntheses are not well defined.[35] Due to uncertainty of the exchange-correction (X-C) functional in the density functional theory (DFT), various X-C functionals have been selected for sulfur in the literature, including the local density approximation (LDA)[36] and the generalized gradient approximation (GGA-PBE)[37] for α-S;[21, 26] the LDA, GGA (both GGA-PBE and GGA-PW91)[37-38] and the hybrid method (e.g. HSE06)[39-40] for $Cu_2ZnSn(S,Se)_4$;[27-31] the LDA and PBE for $Li_{10}GeP_2S_{12}$,[32-33] the LDA for Li_3PS_4[16] and $Li_7P_3S_{11}$,[17] and the PW91 for MoS_2.[41] Since physical and chemical properties of pure sulfur were not well examined and established in the literature, it is difficult to judge the reliability of each X-C functional and hence the aforementioned DFT calculations were performed more or less in isolation.

The present work aims to evaluate the capability of first-principles calculations to predict the structural, phonon, elastic, thermodynamic, and optical properties of the most stable α-S under STP (the focus of the present work) as well as β-S, γ-S, Li_2S, CuS, ZnS, Cu_2ZnSnS_4, SnS, Sn_2S_3, and SnS_2. Specially, the present work answers the following critical questions: (a) What is the best X-C functional for first-principles calculations in sulfur and sulfur-containing materials for different purposes and properties? (b) What is the role of van der Waals interaction in these materials? (c) What are the fundamental physical and chemical properties as well as the quantitative bonding and (non)polar nature in sulfur?

In the present work, structural properties of the aforementioned materials are examined using eight or the presently suggested X-C functionals. Thermodynamic properties are probed using the quasiharmonic approach in terms of phonon calculations (or Debye model for testing purposes).[42] Phonon dispersions and phonon density of states are calculated using a mixed-space approach capable of predicting the LO-TO (longitudinal and transverse optical) zone center splitting.[43] Elastic constants are predicted by an efficient strain-stress method.[44] In Section 2, computational approaches are briefly presented. In Section 3, computed properties of α-S as well as other materials are presented and discussed along with bonding mechanisms of α-S based on the computed force constants and the distribution of charge density. Based on a comparison of the predicted quantities with respect to experimental data, suitable X-C functionals are suggested for practical calculations of α-S as well as S-containing materials. Major conclusions are summarized in the final Section.

2. Computational methodologies

2.1. Structural information for sulfur and sulfides

The focus of the present work is the most stable allotrope of sulfur under STP, i.e., the orthorhombic α-S_8 (α-S) with space group *Fddd* (#70).[2-3] α-S consists of crown-shape S_8 rings, including four kinds of independent atoms located at four different Wyckoff sites 32h. Correspondingly, there are 128 atoms in the crystallographic (conventional) cell and 32 atoms in the primitive cell (see Figure 1, Table S1[†], and Table S2[†] for structural details). In addition to α-S, the other two crystalline phases consisting of S_8 rings are β-S_8 (β-S) and γ-S_8 (γ-S).[2] At low temperatures, ordered β-S possesses a space group of *P2$_1$* (#4) and transfers to a disordered β-S with space group of *P2$_1$/c* (#14) at about 198 K.[2] For simplicity, only the ordered β-S will be

studied in the present work. Regarding the monoclinic γ-S, it has a space group of $P2/c$ (#13),[2]

and its bond lengths are much longer than those in α-S and β-S. In addition to the three sulfur

allotropes consisting of S_8 rings, the S-containing energy materials Li_2S, CuS, ZnS, Cu_2ZnSnS_4

(CZTS), SnS, Sn_2S_3, and SnS_2, along with their constituent elements α-Sn, fcc Cu, bcc Li, and

hcp Zn, were also examined in the present work with their structural details given in Table 2.

2.2. First-principles and phonon calculations

All DFT-based first-principles calculations in the present work were performed using the Vienna

Ab-initio Simulation Package (VASP 5.3.5),[45-46] together with the ion-electron interaction

described by the projector augmented wave (PAW) method.[47] Eight X-C functionals (and

methods) were tested in the present work: (i) the LDA;[36] (ii and iii) the widely used GGA

developed by Perdew-Wang (GGA-PW91)[38] and by Perdew-Burke-Ernzerhof (GGA-PBE);[37] (iv)

the improved PBE for densely packed solids and their surfaces, i.e., the PBEsol (or PS for

simplicity);[48] (v) the revised PBE by Zhang and Yang, i.e., the RP;[49] (vi) the hybrid X-C

functional of Heyd-Scuseria-Ernzerhof (HSE06)[39-40] with 25% nonlocal Hartree-Fock exchange

and 75% semilocal exchange of PBEsol used in the present work; and (vii and viii) the semi-

empirical van der Waals correction as implemented by Grimme et al. (the D3 method),[50] i.e., the

PBE+D3 and the PBEsol+D3 method. Note that PBEsol was included in both the HSE06 and the

D3 methods since it is one of the recommended X-C functionals in the present work (see details

below). In addition, the D3 method was also applied to PBE based on the present tests (see Table

1). Note also that the D3 method was tested previously for structural properties of molecular

crystals by Moellmann and Grimme.[51]

For elemental sulfur, six electrons ($3s^2 3p^4$) were treated as valence electrons. Valence configurations for other elements can be found in our previous publications.[52-53] During VASP calculations, a 360 eV plane wave energy cutoff was generally employed (except for α-Sn). In addition, k-point mesh of 5×7×7 (or 3×3×3 for time-consuming HSE06 calculations) was used for the primitive cell of α-S with 32 atoms. Other k-point meshes and cutoff energies were provided in Table 1 and Table 2. The reciprocal-space energy integration was performed using the Gauss smearing method for structural relaxations and phonon calculations. Final calculations of total energies and electronic structures were performed by the tetrahedron method incorporating a Blöchl correction.[54] The self-consistency of total energy was converged to at least 10^{-6} eV/atom.

Phonon calculations were carried out using the supercell method in terms of the 128-atom cell for α-S (see Figure 1, the k-points mesh is 3×3×1 (or 4×4×1 for test purpose)) and 48-atom cell for β-S (see Table 1, k-mesh is 4×3×3). Force constants, i.e. the Hessian matrix, were calculated directly using the VASP code. Phonon properties were predicted using a parameter-free, mixed-space approach as implemented in the YPHON code.[43, 55] It is worth mentioning that this mixed-space approach was recently developed in our group with force constants computed from the real space (supercell) and the long-range dipole-dipole interactions computed from the reciprocal space, and works well for both polar and nonpolar materials.[43, 55] In the present work, the long-range dipole-dipole interactions including properties of the Born effective charge tensor and dielectric tensor, which result in the LO-TO splitting, were calculated from the linear response method in the reciprocal space (or from the Berry phase approach[56] for the case of the hybrid

functional of HSE06). More details of phonon calculations using the YPHON code can be found in the literature.[43, 53, 55, 57-59]

2.3. First-principles thermodynamics and elasticity

First-principles thermodynamic properties can be predicted using the quasiharmonic approach, i.e., the Helmholtz energy F under volume V and temperature T is determinable by,[42]

$$F(V,T) = E(V) + F_{vib}(V,T) + F_{el}(V,T) \tag{1}$$

Here, $F_{el}(V,T)$ is the thermal electronic contribution estimated from the electronic density of state (DOS). This term is important for metals with non-zero electrons at the Fermi level, and was ignored herein since all the materials of interest (α-S and β-S) are semiconductors. $F_{vib}(V, T)$ is the vibrational contribution to F, which can be determined from phonon DOS (at least 5 volumes used herein) or Debye model (see details in ESI†).[42] The term $E(V)$ is the static energy at 0 K without the zero-point vibrational energy (ZPE).[53] This term is determinable by fitting the first-principles E-V data points according to a four-parameter Birch-Murnaghan equation of state (EOS),[42]

$$E(V) = a_1 + a_2 V^{-2/3} + a_3 V^{-4/3} + a_4 V^{-2} \tag{2}$$

where a_1, a_2, a_3, and a_4 are fitting parameters. Correspondingly, the pressure-volume (P-V) EOS can be obtained by $P = -\partial E / \partial V$, i.e.

$$P(V) = (2/3)a_2 V^{-5/3} + (4/3)a_3 V^{-7/3} + 2a_4 V^{-3} \tag{3}$$

Equilibrium properties estimated from both the E-V EOS and the P-V EOS include the volume V_0, the bulk modulus B_0, and the pressure derivative of bulk modulus B_0', plus the equilibrium energy E_0.[42] At least six reliable data points were used to estimate the parameters for each EOS in the present work.

Regarding elastic constants c_{ij}'s for the orthorhombic α-S, nine independent c_{ij}'s exist. Here, an efficient strain-stress method developed by the present authors[44] was employed. The non-zero values of ±0.007, ±0.01, and ±0.013 were adopted for each set of strains. More details about first-principles elastic constants and the format of the employed sets of strains are available in the literature.[44, 60-61]

3. Results and discussion

3.1. Structural and optical properties of α-S

Table 1 summarizes the structural properties of α-S predicted by the *E-V* EOS (Equation 2) and the *P-V* EOS (Equation 3) in terms of eight X-C functionals: LDA,[36] PBEsol,[48] PBEsol+D3,[50] HSE06,[39-40] PW91,[38] PBE,[37] PBE+D3,[50] and RP.[49] It is noted that the *P-V* EOS predicts a smaller V_0 but a larger B_0 in comparison with those from the *E-V* EOS. Note also that a large difference of V_0 (as well as B_0) between predictions from the *P-V* EOS and from the *E-V* EOS is a signal of less accurate calculations, such as the cases from HSE06, PBE, PW91, and RP for α-S (see Table 1). In the present work, the properties from the *E-V* EOS are mainly employed, unless otherwise stated. Similar to the observations for bcc Fe with dilute oxygen,[62] computed values of V_0 for α-S follow the trends of LDA < PBEsol+D3 < PBEsol < PBE+D3 < HSE06 << PBE < PW91 << RP. As expected, the van der Waals correction (using the D3 method) reduces the corresponding V_0. Note that the D3 correction was applied to GGA-PBE instead of GGA-PW91, since PBE gives a relatively smaller V_0.

Table 1 as well as Figure 2 indicates that PBEsol is the best X-C functional to predict V_0 with the error < 2% (compared with experiment data,[2, 63] the same below). Another reasonable predictions of V_0 are from PBEsol+D3 (-9% smaller) and PBE+D3 (6% larger). However, the normal GGA (both PBE and PW91) and the improved one of RP are worse selections to predict V_0 with the errors > 45%. Computed V_0 from LDA is smaller than experimental data[2, 63] with the error about -13%. HSE06 gives also reasonable but larger V_0 (or smaller V_0 from the P-V EOS). However, the hybrid functional of HSE06 is a time-consuming calculation. Regarding the values of V_0 predicted from the E-V EOS and the P-V EOS, smaller differences (< 3%) are found for results from LDA, PBEsol, PBEsol+D3, and PBE+D3. While calculations using the other X-C functionals are less reliable with the predicted V_0 differences > 9% (see Table 1 and Figure 2). From the predicted lattice parameters and Wyckoff sites in comparison with experimental data[63] (see Table S1† and Table S2†), it is found that the predictions from PBEsol are also better than those from LDA, PBEsol+D3, and PBE+D3. However, structural properties from these three X-C functionals are also acceptable to some extent, especially for the case of PBE+D3.

Regarding the computed B_0 of α-S at its theoretical equilibrium volumes, Table 1 as well as Figure 2 shows that the PBEsol+D3 method predicts the best B_0 in comparison with experimental data[64-66] (around 10.6 GPa, see Table 1 for details). Other reasonable predictions are from LDA, PBEsol, and PBE+D3. It seems that the value of B_0 from HSE06 in terms of the P-V EOS is the most reasonable one (error -3%). However, HSE06 in terms of the E-V EOS predicts a much smaller B_0 (error -71%). Opposite to the V_0 case, the PBE, PW91, and RP predict a very small B_0 with errors around -95% (see Table 1 and Figure 2). About the pressure derivative of bulk modulus, B_0', Table 1 shows that this value is around 7~10 for α-S, which is

larger than the normal value of 3~6,[60] implying a larger thermal expansion of α-S.[67] Note that the measured $B_0' = 7$ was based on four data points at high pressures,[64] which is for reference only but it also agrees more or less with the present predictions. The large value of B_0' is also a main reason regarding the failure of the normal Debye model to predict thermodynamic properties of α-S, see ESI[†].

Table 1 also lists the predicted band gaps of α-S at its theoretical equilibrium volumes. It is seen that the prediction from HSE06 (3.55 eV) agrees well with experimental values (~3.6 eV, see Table 1 for details),[21, 66] and the predictions from PBEsol+D3 (1.78 eV), PBEsol (1.96 eV), and PBE+D3 (2.11 eV) are also reasonable. Note that the predictions from PBE, PW91, and RP are listed for reference only since (i) they predict unreasonably large volumes and (ii) the predicted band gap increases with increasing volume for α-S. As examples, Table 3 lists the predicted macroscopic static dielectric constants from PBEsol, PBE+D3, PBEsol+D3, and HSE06. Similar to the conclusion drew for band gap, dielectric constants calculated from HSE06 agree well with experimental data along different axes.[66] In addition, the other three X-C functionals give also reasonable results, indicating dielectric constants are not sensitive to X-C functional.

In terms of the predicted structural properties as well as band gaps and dielectric constants of α-S, it is conclusive that the D3 method (PBEsol+D3 and PBE+D3), PBEsol, and LDA are practical selections by considering both accuracy and computational efficiency; moreover, HSE06 predicts very accurate optical properties including band gap and dielectric constants. Hence, these four X-C functionals (PBEsol, PBEsol+D3, PBE+D3, and LDA) will be examined further.

3.2. Phonon properties and bonding characteristics of α-S

At the Brillouin zone center (Γ point) of α-S with space group *Fddd*, four Wyckoff sites of 32h (see Table S2[†]) possess the following mechanical representation of vibrational modes,

$$12A_g(R) + 12B_{1g}(R) + 12B_{2g}(R) + 12B_{3g}(R) + 12B_{1u}(IR) + 12B_{2u}(IR) + 12B_{3u}(IR) + 12A_u \quad (4)$$

Hence, α-S has 48 Raman (R) active modes, 36 infrared (IR) active modes, and 12 silent (inactive) modes. Three acoustic modes are B_{1u}, B_{2u}, and B_{3u}. These 96 modes at Γ point predicted from PBEsol, PBE+D3, PBEsol+D3, and LDA are listed in Table S3[†] together with available measurements.[68] It is found that these four X-C functionals predict similar phonon modes, which agree reasonably well with experimental data. For example, the maximum frequency from measurement (476 cm^{-1})[68] agrees with the predictions (around 470~480 cm^{-1}, see Figure 3, Figure S1[†], and Table S3[†]). It is worth mentioning that no apparent differences exist for the predicted frequencies of α-S with and without the consideration of LO-TO splitting. For example, the maximum difference is less than 1 cm^{-1} for a B_{2u} mode with frequency of 226 cm^{-1} (from PBEsol, see Table S3[†] for details). Here, the employed Born effective charge tensor and dielectric tensor for phonon calculations were predicted using HSE06 based on the structure relaxed by PBEsol (see Table 3 for the predicted dielectric constants). The negligible effect of LO-TO splitting indicates that α-S is almost a non-polar crystal, therefore, the LO-TO splitting is ignored in the present work for other phonon calculations.

As examples, Figure 3 shows the predicted phonon dispersions and phonon DOS of α-S at its theoretical equilibrium volumes in terms of PBEsol and PBEsol+D3 (see Table 1). Measured frequencies at Γ point (see Table S3[†])[68] by Raman and infrared spectra are also shown for

comparison. A reasonable agreement is found between experiments and predictions except for the measured frequency of 424 cm^{-1}, since a forbidden phonon region is predicted from around 400 to 450 cm^{-1}. In addition, Figure 3 shows that the maximum frequency is about 480 cm^{-1} from both the predictions and the measurements, and the largest forbidden phonon gap is from around 250 to 370 cm^{-1}. Similar predictions and conclusions also can be drawn from LDA and PBE+D3 (see Figure S1[†]). Regarding phonon DOS, it is shown (see Figure S2[†]) that PBEsol, PBEsol+D3, and LDA predict similar results, which are different from that of PBE+D3. It is observed that at the low frequency region (< 100 cm^{-1}) the phonon densities from high to low follow the trend of PBEsol > PBE+D3 > PBEsol+D3 > (but $\approx$) LDA. This indicates that a softer α-S is predicted from PBEsol among these four functionals (see also bulk moduli in Table 1 as well as Figure 2), and in turn, a faster increase of entropy with increasing temperature will be resulted from PBEsol, since vibrational entropy is proportional to phonon DOS as follows [69]

$$S \propto \int g(\omega)\ln(\omega)d\omega \qquad (5)$$

where ω is the frequency and g(ω) the phonon DOS.

Force constants from phonon calculations allow quantitative analysis of the interactions between atomic pairs.[53, 57, 70] A strong interaction between atomic pair is indicated by a large and positive force constant, while a negative force constant indicates that the atomic pair tends to separate from each other. As an example, key variations of the reduced force constants, i.e., the stretching force constants (SFC's), are plotted in Figure 4 predicted from PBEsol. As expected, the largest SFC's (about 10 eV/Å^2) are for the nearest atomic pairs ($\sim$2.05 Å) within the S$_8$ ring (see atomic pairs 1-2, 2-3, 3-4, and so on in Figure 1), and the second largest SFC's (about 2.7 eV/Å^2) are for the second nearest atomic pairs ($\sim$3.35 Å) within the S$_8$ ring (see atomic pairs 1-3 and 2-4 etc in

Figure 1). For atomic pairs between the S_8 rings with bond lengths from 3.4 to 5.4 Å and the SFC's around 0.1-0.2 eV/Å^2 (representing the van der Waals forces), they possess the similar SFC values as those for the third nearest atomic pairs within the S_8 rings (atomic pairs 1-4 and 2-5 etc in Figure 1) and play a crucial role to connect the S_8 rings.

The strong interactions within the S_8 ring of α-S are also indicated by the charge density difference contours shown in Figure 1. They are computed from the difference between the charge density after electronic relaxations and the non-interacting charge density from one electronic step,[71] indicating the charge density redistribution upon formation of the orthorhombic α-S. Between the S_8 rings, the charge gains and losses are negligible and therefore they are ignored in Figure 1. The charge gains in Figure 1 indicate the strong interactions within the S_8 ring, and the bond directionality between the S-S pairs provides an indication of the covalent character. These interactions are traceable from the *s-p* hybridization, contributed by more electrons in the 3*p* orbital as well as a small part of electrons in the 3*s* orbital, see the partial electronic DOS of α-S in Figure S3[†].

3.3. Elasticity of α-S

Table 4 summarizes the predicted elastic constants c_{ij}'s of α-S from LDA, PBEsol, PBEsol+D3, and PBE+D3 in comparison with experimental data.[65] The error of each c_{ij} is around 0.5 GPa by examining the c_{ij} values from different groups of non-zero strains (±0.007, ±0.01, and ±0.013). Table 4 shows that these c_{ij} values are small (< about 41 GPa), due mainly to the weak van der Walls forces between these S_8 rings (see force constants in Figure 4). The c_{33} value is the largest one, followed by c_{11} and c_{22}, which are consistent with the predicted dielectric constants along

the *a*-, *b*-, and *c*-axis directions (see Table 3). Except for c_{11}, c_{22}, and c_{33}, the relatively large values are for c_{44} (i.e., c_{2323} or c_{3232} etc in the format of the fourth-rank tensors) and c_{23} with respect to the others (c_{55}, c_{66}, c_{12}, and c_{13}). Figure 5 plots the predicted c_{ij}'s in comparison with experimental data.[65] Similar to the observation for bulk modulus from EOS fitting (see Table 1), the D3 method gives a better c_{ij} prediction, and the experimental elastic properties are roughly in the middle of the predictions from PBE+D3 and PBEsol+D3. In addition, LDA and PBEsol give also a reasonable c_{ij} prediction.

In terms of the single crystal c_{ij}'s and the Hill approach,[61, 72] Table 4 shows also the polycrystalline aggregate properties of bulk modulus (*B*), shear modulus (*G*), Young's modulus (*Y*), and Poisson's ratio (ν). The predicted values of B_{Hill} from c_{ij}'s (4.2, 6.8, 12.9, and 15.2 GPa from PBEsol, PBE+D3, PBEsol+D3, and LDA, respectively) agree well but slightly smaller than those from the EOS fittings (B_0, see Table 1). Similar to B_{Hill} and B_0, measured values of G_{Hill} and Y_{Hill} are also roughly in the middle of the predictions by PBEsol+D3 and PBE+D3. Regarding the Poisson's ratio ν_{Hill}, the predictions (in particular from PBEsol) are smaller than the measurements due mainly to a smaller *B*/*G* ratio, since

$$\nu = \frac{3B-2G}{6B+2G} = \frac{1}{2} - \frac{1}{\frac{2B}{G}+\frac{2}{3}} \tag{6}$$

Based on Poisson's ratio (calculated from c_{ij}'s) and equilibrium properties of bulk modulus and volume, Debye temperature at a given volume can be predicted (see details in ESI† as well as the literature[42, 73-74]). Table 4 lists the Debye temperatures (Θ_0) of α-S at its equilibrium volumes from first-principles calculations and experiments.[65] The Θ_0 values from elasticity are roughly 200 K (170-258 K), which are only half of the second moment Debye temperature (510~520 K)

predicted from phonon DOS (in terms of PBEsol, PBE+D3, PBEsol+D3, and LDA).[42] The

scattered Debye temperatures from predictions (~200 and ~520 K) agree reasonably well with

experimental results for α-S (187.5,[65] 250,[66] and 520 K[75]).

3.4. Thermodynamic properties of α-S

Figure 6 illustrates the predicted thermodynamic properties of α-S up to 370 K under external

pressure $P = 0$ GPa using the quasiharmonic phonon approach of Equation (1), including

enthalpy (equals to internal energy due to $P = 0$), entropy, and Gibbs energy (equals to

Helmholtz energy at $P = 0$). Here, the enthalpy is set to zero at 298.15 K, i.e., the same as the

standard element reference used in the CALPHAD community.[76-77] Each figure is terminated at

370 K, which is close to the phase transition temperature of α-S to a high temperature phase of

β-S.[2, 76] Figure 6 shows that the predictions from LDA and PBEsol+D3 agree well with the

Scientific Group Thermodata Europe (SGTE) data[76] evaluated based on experimental data, while,

the predictions from PBEsol and PBE+D3 agree reasonably with the SGTE data due to the faster

increase of vibrational entropy with temperature, see Figure S2† and the reason shown in

Equation (5).

Regarding thermodynamic properties which are the second derivatives of Gibbs energy (or

Helmholtz energy due to $P = 0$ GPa), Figure 7 illustrates the heat capacity at constant pressure

(C_P) and the linear thermal expansion coefficient (TEC) of α-S calculated by the quasiharmonic

phonon approach in terms of LDA, PBEsol, PBEsol+D3, and PBE+D3. SGTE data[76] and

experimental data[66, 78] are also plotted for comparison. For C_P, all these four X-C functionals

give a good prediction, espeically the results from LDA and PBEsol+D3. Regarding the linear

TEC, the best prediciton is from PBEsol+D3. Note that these TEC predicitons are consistent with the above observation: a softer α-S crystal (from such as PBEsol and PBE+D3) corresponds to a larger vibrational entropy contribution, and in turn, a larger TEC.

According to the predicted thermodynamic properties of α-S as shown in Figure 6 and Figure 7, it is conclusive that PBEsol+D3 is the best X-C functional. Moreover, phonon properties of α-S from PBEsol+D3 should be the most accurate predictions, at least in the low frequency region (see the reason given by Equation 5). For comparison, it is also interesting to see how good the thermodynamic properties of α-S predicted from the Debye model[42] (see ESI[†] for details). As mentioned above, Debye temperatures of α-S are scattered. In addition, Table 1 indicates that α-S is an unusual crystal with large B_0' (7~10) and small B_0 (around 10 GPa). Test calculations show that the normal settings of the Debye-Grüneisen model[42] cannot describe the thermodynamic properties of α-S due to a rapid change of Debye temperature with increasing volume (see ESI[†] for details). Since this rapid change is due mainly to the large B_0', and in turn, the large Grüneisen constant (see ESI[†]). Hence, we suggest that the Grüneisen constant can be treated as an adjustable parameter in the Debye-Grüneisen model[42] in order to describe the "slow" change of Debye temperature with respect to the change of volume (see details in ESI[†]). Accordingly, a roughly reliable prediction of thermodynamic properties can be obtained for α-S (see Figure S4[†]). It is expected that the present suggestion also works for other unusual materials with large B_0' (such as > 7) and small B_0 (such as < 50 GPa).

3.5. Test of structural and thermodynamic properties of β-S, γ-S, and sulfides

Based on the results from α-S, the suggested X-C functional is PBEsol+D3 as well as PBE+D3 and PBEsol. Further examination of these functionals is summarized in Table 2 for β-S, γ-S, and the energy-related metal sulfides of Li_2S, CuS, ZnS, CZTS, SnS, Sn_2S_3, and SnS_2. The enthalpy of formation (ΔH), equilibrium volume (V_0), bulk modulus (B_0) and its pressure derivative (B_0') were predicted at 0 K using the *E-V* EOS (see Equation 2) without considering the ZPE. Available experimental data[60, 63, 79-92] are also listed for comparison in Table 2. Note that (i) the reference states of ΔH are α-S and the pure elements listed in Table 2; (ii) the measured B_0' was -2±2 for covellite CuS,[82] but other first-principles results (4~5)[93] agree with the present value near 5; (iii) direct measurement of ΔH is not available for CZTS, other first-principles results were from -42.1 to -50.8 kJ/mole-atom,[29, 94-95] and an indirect value based on the sputtering rates measurement was -116±12 kJ/mole-atom for $Cu_{1.9}Zn_{1.5}Sn_{0.8}S_4$,[85] which is far from the present and other first-principles predictions maybe due to the large composition difference; and (iv) direct measurement of B_0 is not available for CZTS, the estimated B_0 of 83.6 GPa[96] was based on an empirical relation for chalcopyrite compounds.[97]

Similar to the conclusion drawn for α-S, Table 1 as well as Figure 8 shows that PBEsol is the best X-C functional to predict V_0 for both β-S and γ-S, and PBEsol+D3 gives the best prediction of ΔH for β-S (followed by LDA). It is found that PBEsol gives a wrong prediction of ΔH for β-S, and the ΔH value from PBE+D3 is too small. Table 2 as well as Figure 8 also shows that PBE+D3 as well as PBEsol gives a good V_0 prediction for sulfides (Li_2S, CuS, ZnS, CZTS, SnS, Sn_2S_3, and SnS_2), and PBEsol+D3 predicts a better B_0 and especially ΔH for these sulfur and sulfides. It should be remarked that the measured values of B_0' are usually based on the scattered

data at high pressures, which should not be set as benchmark to judge the quality of first-principles calculations.

At finite temperatures, Gibbs energy difference (ΔG) between the ordered β-S and α-S is shown in Figure S5[†] based on the PBEsol+D3 method and the quasiharmonic phonon approach of Equation 1. It is found that the predicted ΔG decreases with increasing temperature becauses of more phonon density for the ordered β-S with respect to that of α-S in the low frequency region (such as < 50 cm^{-1}, see Figure S6[†] and the reason shown in Equation 5). The predicted phase transition temperature between the ordered β-S and α-S is greater than 700 K, much higher than the measurement value of 368 $K^{[2]}$, but this temperature is quite reasonable because of (i) the ignorance of phase transition between the ordered and disordered β-S at about 198 K,[2] and (ii) the omission of configurational entropy for the disordered β-S. Regarding sulfides, we tested the anti-fluorite Li_2S in terms of the quasiharmonic phonon approach, similar to the case of α-S the best thermodynamic properties in comparison with experiments are also resulted from the van der Waals correction (PBE+D3 or PBEsol+D3), see details in other publication.[98]

These examinations validate further the conclusion drawn for α-S, i.e., the van der Waals correction is crucial to predict the properties of sulfur and S-containing materials, and the suggested X-C functional is PBEsol+D3 as well as PBE+D3 and maybe PBEsol for some cases.

It should be remarked that the calculated structural properties at 0 K and without the effect of ZPE are presented in Table 1 and Table 2, and Figure 2 and Figure 8, however, experimental data are usually measured at room temperature (298 K). As examples, Table S4[†] shows the

predicted V_0 and B_0 for two materials at 0 K (with and without the effect of ZPE) and room temperature (298 K): an unusual material of α-S with $B_0' > 7$ and a normal material of Li$_2$S with $B_0' \sim 4$. The general trend shown in Table S4[†] is that the calculated V_0 at 298 K is about 2-4% larger than the V_0 at 0 K and without ZPE. The trend for B_0 is slightly complicated. It is seen that the calculated B_0 at 298 K decreases about 6-9% for a normal material such as Li$_2$S in comparison with the B_0 at 0 K and without ZPE. However, the decrease of B_0 is more than 10% for an unusual material for example of α-S. Note also that the structural properties at room temperature will not change the conclusions drew from Table 1, Table 2, Figure 2, and Figure 8. However, the general difference of structural properties between 0 K (without ZPE) and room temperature should be kept in mind when compared to experimental data.

4. Conclusions

A comprehensive first-principles study based on the density functional theory has been performed to examine the structural, phonon, elastic, thermodynamic, and optical properties of the orthorhombic α-S with space group *Fddd* by using a variety of exchange-correction (X-C) functionals and the van der Waals correction in terms of the D3 method. Further examination is also performed for β-S and γ-S and the energy-related metal sulfides of Li$_2$S, CuS, ZnS, Cu$_2$ZnSnS$_4$ (CZTS), SnS, Sn$_2$S$_3$, and SnS$_2$. In comparison with experimental data, it is found that (a) the best X-C functional to predict the structural properties of α-S is an improved GGA of PBEsol, while the worse selections are GGA-PW91, GGA-PBE, and GGA-RP; (b) the hybrid X-C functional of HSE06 is a good selection to predict the optical and electronic properties of α-S such as the band gap and dielectric constants; (c) phonon and elastic properties of α-S can be predicted reasonably well using LDA and PBEsol and in particular using the PBE+D3 and the

PBEsol+D3 method; (d) the PBEsol+D3 method is the best X-C functional to compute the thermodynamic properties of α-S in terms of the quasiharmonic phonon approach, and the other reasonable functionals for this purpose are LDA as well as PBE+D3 and PBEsol. It is also possible to use a revised Debye model to predict the less-accurate results for unusual materials such as α-S. The present work demonstrates the crucial role of van der Waals correction for sulfur and S-containing compounds, making the suggested X-C functionals being PBEsol+D3 and PBE+D3 (and PBEsol in some cases) for first-principles study of these materials. In addition, the strong interactions within the S_8 ring of α-S and the weak van der Waals interactions between these S_8 rings are also revealed quantitatively from phonon force constants and qualitatively from the differential charge density.

Acknowledgements

References

1.   N. S. Lewis and D. G. Nocera, *Proc. Nat. Aca. Sci. U.S.A.*, 2006, **103**, 15729.
2.   R. Steudel and B. Eckert, *Top. Curr. Chem.*, 2003, **230**, 1.
3.   B. Meyer, *Chem. Rev.*, 1976, **76**, 367.
4.   M. R. Gao, Y. F. Xu, J. Jiang and S. H. Yu, *Chem. Soc. Rev.*, 2013, **42**, 2986.
5.   X. H. Rui, H. T. Tan and Q. Y. Yan, *Nanoscale*, 2014, **6**, 9889.
6.   S. R. Kodigala, *Thin Film Solar Cells From Earth Abundant Materials: Growth and Characterization of Cu₂ZnSn(SSe)₄ Thin Films and Their Solar Cells*, Elsevier, New York, 2014.
7.   D. J. Milliron, *Nat. Mater.*, 2014, **13**, 772.
8.   B. Yang, L. Wang, J. Han, Y. Zhou, H. B. Song, S. Y. Chen, J. Zhong, L. Lv, D. M. Niu and J. Tang, *Chem. Mat.*, 2014, **26**, 3135.
9.   S. J. Fredrick and A. L. Prieto, *J. Am. Chem. Soc.*, 2013, **135**, 18256.
10.   X. S. Fang, T. Y. Zhai, U. K. Gautam, L. Li, L. M. Wu, B. Yoshio and D. Golberg, *Prog. Mater. Sci.*, 2011, **56**, 175.
11.   P. G. Bruce, S. A. Freunberger, L. J. Hardwick and J.-M. Tarascon, *Nat. Mater.*, 2012, **11**, 19.
12.   R. Van Noorden, *Nature*, 2014, **507**, 26.
13.   N. Kamaya, K. Homma, Y. Yamakawa, M. Hirayama, R. Kanno, M. Yonemura, T. Kamiyama, Y. Kato, S. Hama, K. Kawamoto and A. Mitsui, *Nat. Mater.*, 2011, **10**, 682.
14.   G. Sahu, Z. Lin, J. C. Li, Z. C. Liu, N. Dudney and C. D. Liang, *Energy Environ. Sci.*, 2014, **7**, 1053.
15.   S. Teragawa, K. Aso, K. Tadanaga, A. Hayashi and M. Tatsumisago, *J. Mater. Chem. A*, 2014, **2**, 5095.
16.   N. D. Lepley, N. A. W. Holzwarth and Y. A. Du, *Phys. Rev. B*, 2013, **88**, 104103.
17.   N. D. Lepley and N. A. W. Holzwarth, *J. Electrochem. Soc.*, 2012, **159**, A538.
18.   G. Sahu, E. Rangasamy, J. C. Li, Y. Chen, K. An, N. Dudney and C. D. Liang, *J. Mater. Chem. A*, 2014, **2**, 10396.
19.   Z. Q. Liu, Y. F. Tang, Y. M. Wang and F. Q. Huang, *J. Power Sources*, 2014, **260**, 264.
20.   A. Sakuda, A. Hayashi and M. Tatsumisago, *Chem. Mat.*, 2010, **22**, 949.
21.   G. Liu, P. Niu, L. Yin and H.-M. Cheng, *J. Am. Chem. Soc.*, 2012, **134**, 9070.
22.   M. S. Faber, R. Dziedzic, M. A. Lukowski, N. S. Kaiser, Q. Ding and S. Jin, *J. Am. Chem. Soc.*, 2014, **136**, 10053.
23.   W. Z. Wu, L. Wang, Y. L. Li, F. Zhang, L. Lin, S. M. Niu, D. Chenet, X. Zhang, Y. F. Hao, T. F. Heinz, J. Hone and Z. L. Wang, *Nature*, 2014, **514**, 470.
24.   H. I. Karunadasa, E. Montalvo, Y. J. Sun, M. Majda, J. R. Long and C. J. Chang, *Science*, 2012, **335**, 698.
25.   O. Lopez-Sanchez, D. Lembke, M. Kayci, A. Radenovic and A. Kis, *Nat. Nanotechnol.*, 2013, **8**, 497.
26.   O. Dieguez and N. Marzari, *Phys. Rev. B*, 2009, **80**, 214115.
27.   A. Walsh, S. Y. Chen, S. H. Wei and X. G. Gong, *Adv. Energy Mater.*, 2012, **2**, 400.
28.   J. Paier, R. Asahi, A. Nagoya and G. Kresse, *Phys. Rev. B*, 2009, **79**, 115126.
29.   T. Maeda, S. Nakamura and T. Wada, *Jpn. J. Appl. Phys.*, 2011, **50**, 04dp07.
30.   S. Y. Chen, J. H. Yang, X. G. Gong, A. Walsh and S. H. Wei, *Phys. Rev. B*, 2010, **81**, 245204.

31.   A. Khare, B. Himmetoglu, M. Cococcioni and E. S. Aydil, *J. Appl. Phys.*, 2012, **111**, 123704.
32.   Y. F. Mo, S. P. Ong and G. Ceder, *Chem. Mat.*, 2012, **24**, 15.
33.   C. H. Hu, Z. Q. Wang, Z. Y. Sun and C. Y. Ouyang, *Chem. Phys. Lett.*, 2014, **591**, 16.
34.   C. R. A. Catlow, Z. X. Guo, M. Miskufova, S. A. Shevlin, A. G. H. Smith, A. A. Sokol, A. Walsh, D. J. Wilson and S. M. Woodley, *Philos. Trans. Roy. Soc. A*, 2010, **368**, 3379.
35.   S. L. Shang and Z. K. Liu, *Appl. Phys. Lett.*, 2007, **90**, 091914.
36.   J. P. Perdew and A. Zunger, *Phys. Rev. B*, 1981, **23**, 5048.
37.   J. P. Perdew, K. Burke and M. Ernzerhof, *Phys. Rev. Lett.*, 1996, **77**, 3865.
38.   J. P. Perdew, J. A. Chevary, S. H. Vosko, K. A. Jackson, M. R. Pederson, D. J. Singh and C. Fiolhais, *Phys. Rev. B*, 1992, **46**, 6671.
39.   J. Heyd, G. E. Scuseria and M. Ernzerhof, *J. Chem. Phys.*, 2003, **118**, 8207.
40.   J. Heyd, G. E. Scuseria and M. Ernzerhof, *J. Chem. Phys.*, 2006, **124**, 219906.
41.   Y. F. Li, Z. Zhou, S. B. Zhang and Z. F. Chen, *J. Am. Chem. Soc.*, 2008, **130**, 16739.
42.   S. L. Shang, Y. Wang, D. Kim and Z. K. Liu, *Comput. Mater. Sci.*, 2010, **47**, 1040.
43.   Y. Wang, J. J. Wang, W. Y. Wang, Z. G. Mei, S. L. Shang, L. Q. Chen and Z. K. Liu, *J. Phys.-Condens. Matter*, 2010, **22**, 202201.
44.   S. L. Shang, Y. Wang and Z. K. Liu, *Appl. Phys. Lett.*, 2007, **90**, 101909.
45.   G. Kresse and J. Furthmuller, *Phys. Rev. B*, 1996, **54**, 11169.
46.   G. Kresse and J. Furthmuller, *Comput. Mater. Sci.*, 1996, **6**, 15.
47.   G. Kresse and D. Joubert, *Phys. Rev. B*, 1999, **59**, 1758.
48.   J. P. Perdew, A. Ruzsinszky, G. I. Csonka, O. A. Vydrov, G. E. Scuseria, L. A. Constantin, X. Zhou and K. Burke, *Phys. Rev. Lett.*, 2008, **100**, 136406.
49.   Y. K. Zhang and W. T. Yang, *Phys. Rev. Lett.*, 1998, **80**, 890.
50.   S. Grimme, J. Antony, S. Ehrlich and H. Krieg, *J. Chem. Phys.*, 2010, **132**, 154104.
51.   J. Moellmann and S. Grimme, *Phys. Chem. Chem. Phys.*, 2010, **12**, 8500.
52.   S. L. Shang, Y. Wang, G. Lindwall, N. R. Kelly, T. J. Anderson and Z. K. Liu, *J. Phys. Chem. C* 2014, **118**, 24884.
53.   S. L. Shang, Y. Wang, Z. G. Mei, X. D. Hui and Z. K. Liu, *J. Mater. Chem.*, 2012, **22**, 1142.
54.   P. E. Blöchl, O. Jepsen and O. K. Andersen, *Phys. Rev. B*, 1994, **49**, 16223.
55.   Y. Wang, S. Shang, Z.-K. Liu and L.-Q. Chen, *Phys. Rev. B*, 2012, **85**, 224303.
56.   R. W. Nunes and X. Gonze, *Phys. Rev. B*, 2001, **63**, 155107.
57.   S.-L. Shang, L. G. Hector, Jr., S. Shi, Y. Qi, Y. Wang and Z.-K. Liu, *Acta Mater.*, 2012, **60**, 5204.
58.   Y. Wang, H. Fang, C. L. Zacherl, Z. Mei, S. Shang, L.-Q. Chen, P. D. Jablonski and Z.-K. Liu, *Surf. Sci.*, 2012, **606**, 1422.
59.   Y. Wang, L. A. Zhang, S. Shang, Z.-K. Liu and L.-Q. Chen, *Phys. Rev. B*, 2013, **88**, 024304.
60.   S. L. Shang, A. Saengdeejing, Z. G. Mei, D. E. Kim, H. Zhang, S. Ganeshan, Y. Wang and Z. K. Liu, *Comput. Mater. Sci.*, 2010, **48**, 813.
61.   S. Ganeshan, S. L. Shang, Y. Wang and Z. K. Liu, *Acta Mater.*, 2009, **57**, 3876.
62.   S. L. Shang, H. Z. Fang, J. Wang, C. P. Guo, Y. Wang, P. D. Jablonski, Y. Du and Z. K. Liu, *Corros. Sci.*, 2014, **83**, 94.
63.   P. Villars and L. D. Calvert, *Pearson's handbook of crystallographic data for intermetallic phases*, ASTM International, Newbury, OH, 1991.

64. H. Luo and A. L. Ruoff, *Phys. Rev. B*, 1993, **48**, 569.

65. G. A. Saunders, Y. K. Yogurtcu, J. E. Macdonald and G. S. Pawley, *Proc. R. Soc. London Ser. A-Math. Phys. Eng. Sci.*, 1986, **407**, 325.

66. O. Madelung, U. Rössler and M. Schulz, eds., *Non-Tetrahedrally Bonded Elements and Binary Compounds I, Landolt-Börnstein-Group III Condensed Matter*, vol. 41C, Springer-Verlag: Heidelberg, Germany, 1998.

67. S. Shang, A. J. Bottger, M. P. Steenvoorden and M. W. J. Craje, *Acta Mater.*, 2006, **54**, 2407.

68. B. Eckert and R. Steudel, *Top. Curr. Chem.*, 2003, **231**, 31.

69. S. L. Shang, Y. Wang, Y. Du and Z. K. Liu, *Intermetallics*, 2010, **18**, 961.

70. S. L. Shang, L. G. Hector, Y. Wang, H. Zhang and Z. K. Liu, *J. Phys.-Condens. Matter*, 2009, **21**, 246001.

71. S. L. Shang, W. Y. Wang, B. C. Zhou, Y. Wang, K. A. Darling, L. J. Kecskes, S. N. Mathaudhu and Z. K. Liu, *Acta Mater.*, 2014, **67**, 168.

72. R. Hill, *Proc. Phys. Soc. London Sec. A*, 1952, **65**, 349.

73. Q. Chen and B. Sundman, *Acta Mater.*, 2001, **49**, 947.

74. X. L. Liu, B. K. VanLeeuwen, S. L. Shang, Y. Du and Z. K. Liu, *Comput. Mater. Sci.*, 2014, In press.

75. C. Y. Ho, R. W. Powell and P. E. Liley, *J. Phys. Chem. Ref. Data*, 1974, **3** (Suppl. 1), 1.

76. A. T. Dinsdale, *CALPHAD*, 1991, **15**, 317.

77. Z.-K. Liu, *J. Phase Equilib. Diff.*, 2009, **30**, 517.

78. R. K. Kirby, T. A. Hahn and B. D. Rothrock, Thermal expansion, in *American Institute of Physics Handbook*, McGraw-Hill, New York, 1972.

79. Scientific Group Thermodata Europe (SGTE), ed., *Thermodynamic Properties of Inorganic Materials*, vol. 19, Springer, Berlin, 1999.

80. W. Buehrer, F. Altorfer, J. Mesot, H. Bill, P. Carron and H. G. Smith, *J. Phys. Condens. Matter*, 1991, **3**, 1055.

81. A. Grzechnik, A. Vegas, K. Syassen, I. Loa, M. Hanfland and M. Jansen, *J. Solid State Chem.*, 2000, **154**, 603.

82. S. M. Peiris, J. S. Sweeney, A. J. Campbell and D. L. Heinz, *J. Chem. Phys.*, 1996, **104**, 11.

83. J. C. Jamieson and H. H. Demarest, *J. Phys. Chem. Solids*, 1980, **41**, 963.

84. S. Desgreniers, L. Beaulieu and I. Lepage, *Phys. Rev. B*, 2000, **61**, 8726.

85. S. V. Baryshev and E. Thimsen, *Enthalpy of formation for Cu-Zn-Sn-S (CZTS), arXiv: 1403.4922v1*, 2014.

86. L. Ehm, K. Knorr, P. Dera, A. Krimmel, P. Bouvier and M. Mezouar, *J. Phys. Condens. Matter*, 2004, **16**, 3545.

87. K. Knorr, L. Ehm, M. Hytha, B. Winkler and W. Depmeier, *Phys. Status Solidi B*, 2001, **223**, 435.

88. C. J. Buchenauer, M. Cardona and F. H. Pollak, *Phys. Rev. B*, 1971, **3**, 1243.

89. A. Dewaele, P. Loubeyre and M. Mezouar, *Phys. Rev. B*, 2004, **70**, 094112.

90. G. Simmons and H. Wang, *Single crystal elastic constants and calculated aggregate properties*, MIT press, Cambridge (Mass.), 1971.

91. B. Olinger and J. W. Shaner, *Science*, 1983, **219**, 1071.

92. T. Kenichi, *Phys. Rev. B*, 1997, **56**, 5170.

93.   A. Morales-Garcia, A. L. Soares, Jr., E. C. Dos Santos, H. A. de Abreu and H. A. Duarte, *J. Phys. Chem. A*, 2014, **118**, 5823.
94.   T. Maeda, S. Nakamura and T. Wada, *Mater. Res. Soc. Symposium Proceedings*, 2009, **1165**, M0403.
95.   S. Chen, J.-H. Yang, X. G. Gong, A. Walsh and S.-H. Wei, *Phys. Rev. B*, 2010, **81**, 245204.
96.   A. Nagaoka, K. Yoshino, K. Aoyagi, T. Minemoto, Y. Nose, T. Taniyama, K. Kakimoto and H. Miyake, *J. Crys. Growth*, 2014, **393**, 167.
97.   J. B. Caceres and C. Rincon, *Phys. Status Solidi B*, 2002, **234**, 541.
98.   S. L. Shang, Y. Wang and Z. K. Liu, *Mater. China*, 2015, In press.

Tables and Table Captions

Table 1

Calculated structural properties of α-S, β-S, and γ-S in terms of various X-C functionals, including the enthalpy of formation (ΔH with the reference state being α-S in kJ/mol-atom), the equilibrium volume (V_0, Å^3/atom), bulk modulus (B_0, GPa) and its pressure derivative (B_0'), and the band gap (BG, eV). Note that (i) the percent errors of the calculated V_0 and B_0 with respect to experimental data are also shown; (ii) the values shown in parentheses indicate the results related to the *P-V* EOS, (iii) all the calculated properties are results at 0 K without considering the zero point vibrational energy (ZPE); and (iv) the calculated V_0 and B_0 at room temperature for two examples of α-S and Li$_2$S are given in Table S4[†].

Sulfur and others	Methods	ΔH	V_0	V_0-error (%)	B_0	B_0-error (%)	B_0'	BG
α-S	LDA	0	22.487 (21.851)	-13 (-15)	14.8 (18.2)	40 (72)	8.34	1.57
Fddd (#70) [a]	PBEsol+D3	0	23.509 (23.403)	-9 (-9)	12.1 (12.5)	14 (18)	8.33	1.78
(5×7×7) [b]	PBEsol	0	26.112 (25.369)	1 (-2)	4.2 (5.7)	-60 (-46)	9.86	1.96
32 atoms [c]	PBE+D3	0	27.290 (27.077)	6 (5)	6.3 (6.7)	-41 (-37)	8.03	2.11
	HSE06		27.581 (24.176)	7 (-6)	3.1 (10.3)	-71 (-3)	8.95	3.55
	PBE		37.343 (33.932)	45 (32)	0.6 (1.3)	-94 (-88)	11.07	2.67
	PW91		40.103 (29.666)	56 (15)	0.4 (1.5)	-96 (-86)	7.57	2.70
	RP		50.322 (44.207)	95 (72)	0.4 (1.0)	-96 (-91)	8.39	2.85
	Expt.		25.76 [d]		10.6 [e]		7 [e]	2.75~4.2 [f]
β-S	LDA	0.34	23.112 (22.428)	-9 (-12)	13.6 (17.2)		8.71	1.87
*P*2$_1$ (#4) [a]	PBEsol+D3	0.43	24.201 (23.900)	-5 (-6)	10.9 (12.0)		7.88	2.00
(5×5×5) [b]	PBEsol	-0.06	26.861 (26.047)	5 (2)	4.1 (5.7)		10.69	2.23
48 atoms [c]	PBE+D3	0.02	27.777 (27.303)	9 (7)	6.9 (7.9)		7.29	2.26
	Expt.	0.36 [g]	25.50 [d]					
γ-S	LDA	0.60	22.967 (22.274)	-12 (-15)	12.9 (17.2)		10.02	1.72
*P*2/*c* (#13) [a]	PBEsol+D3	0.47	24.024 (23.736)	-8 (-9)	11.1 (12.3)		7.99	1.88
(7×4×7) [b]	PBEsol	0.09	27.363 (26.102)	4 (0)	2.9 (5.2)		11.34	2.19
32 atoms [c]	PBE+D3	0.10	27.604 (27.093)	5 (3)	6.6 (7.6)		7.95	2.18
	Expt.		26.21 [d]					

[a] Space group and its number in parentheses.

[b] Normal *k*-points mesh used in the present first-principles calculations and the (3×3×3) was used for the time-consuming HSE06 calculations of α-S.

[c] Total atoms in unit cell used in the present first-principles calculations.

[d] Measured lattice parameters (Å) at room temperature:[2, 63] $a = 10.4646$, $b = 12.8660$, and $c = 24.4860$ for α-S; $a = 10.799$, $b = 10.684$, $c = 10.663$, and angle $\beta = 95.71°$ for ordered β-S; $a = 8.455$, $b = 13.052$, $c = 9.267$, and angle $\beta = 124.89°$ for γ-S.

[e] Average bulk modulus according to measurements of 8.0, 11, 12.1 (based on the measured elastic constants, see Table 4),[65] 14.5 (based on four data points at high pressures and the corresponding $B_0' = 7$),[64] 7.7,[65] and 10 GPa.[66]

[f] Measured values[21, 66] and the mean value should be around 3.6 eV.

[g] SGTE value at 298 K estimated based on experimental data,[79] and this value is for disordered β-S (*P*2$_1$/*c*) with respect to α-S.

Table 2

Calculated and experimental properties of S-containing energy materials and their constituent elements, including enthalpy of formation (ΔH, kJ/mole-atom) with respect to pure elements shown in this Table and α-S in Table 1, equilibrium volume (V_0, Å^3/atom), bulk modulus (B_0, GPa) and its pressure derivative (B_0'). Note that the predications are results at 0 K using the *E-V* EOS and without considering the zero point vibrational energy (ZPE), and the calculated V_0 and B_0 at room temperature for two examples of α-S and Li$_2$S are given in Table S4[†].

Materials	Notes	Methods	ΔH	V_0	B_0	B_0'
Li$_2$S	$Fm\overline{3}m$ (# 225) [a]	PBE	-129.6	15.619	40.6	4.06
(anti-fluorite)	(16×16×16) [b]	PBEsol	-129.6	15.188	41.6	4.28
	12 atoms [c]	PBE+D3	-137.1	14.777	46.2	4.24
	360 eV [d]	PBEsol+D3	-135.1	14.567	46.1	3.97
		Expt.	-148.8 [e]	15.50 [f]	45.7±2.7 [g]	2.1±0.4 [h]
					52±2 [h]	
CuS	$P6_3/mmc$ (# 194) [a]	PBE	-19.3	17.317	77.5	4.91
(covellite)	(19×19×4) [b]	PBEsol	-22.4	16.384	93.3	4.88
	12 atoms [c]	PBE+D3	-20.1	16.732	88.7	4.99
	360 eV [d]	PBEsol+D3	-22.2	15.964	103.6	4.86
		Expt.	-27.9 [e]	16.96 [f]	89±10 [i]	-2±2 [i]
ZnS	$F\overline{4}3m$ (# 216) [a]	PBE	-86.1	20.250	69.0	4.41
(zinc blende)	(13×13×13) [b]	PBEsol	-71.4	19.293	78.0	4.49
	8 atoms [c]	PBE+D3	-81.3	19.558	78.1	4.50
	360 eV [d]	PBEsol+D3	-79.4	18.787	85.8	4.46
		Expt.	-102.6 [e]	19.79 [f]	74.8±3.2 [j]	4.91±1.2 [j]
					79.5 [k]	4 [k]
Cu$_2$ZnSnS$_4$	$I\overline{4}$ (# 82) [a]	PBE	-46.7	20.504	67.6	4.85
(kesterite)	(12×12×6) [b]	PBEsol	-45.1	19.491	79.4	4.85
	16 atoms [c]	PBE+D3	-48.4	19.844	78.3	4.82
	360 eV [d]	PBEsol+D3	-48.7	19.025	88.6	4.74
		Expt.	N/A	20.00 [f]	N/A	N/A
			(-42 ~ -50) [l]		(83.6) [m]	
			(-116) [l]			
SnS	$Pnma$ (# 62) [a]	PBE	-43.8	25.422	22.2	10.36
	(7×20×19) [b]	PBEsol	-48.5	23.293	38.2	7.08
	8 atoms [c]	PBE+D3	-48.0	24.597	24.4	11.19
	360 eV [d]	PBEsol+D3	-51.4	22.783	41.0	6.95
		Expt.	-53.8 [e]	23.98 [f]	36.6±0.9 [n]	5.5±0.2 [n]
Sn$_2$S$_3$	$Pnma$ (# 62) [a]	PBE	-39.6	25.430	12.3	14.69
	(6×13×4) [b]	PBEsol	-44.5	22.862	26.1	8.70
	20 atoms [c]	PBE+D3	-44.0	24.035	20.9	9.29
	360 eV [d]	PBEsol+D3	-47.8	22.117	33.1	7.01
		Expt.	-51.9 [e]	23.39 [f]	N/A	N/A
					(32) [o]	
SnS$_2$	$P\overline{3}m1$ (# 164) [a]	PBE	-37.6	26.270	6.5	14.85
	(22×22×12) [b]	PBEsol	-42.5	23.316	14.5	13.95
	3 atoms [c]	PBE+D3	-41.4	23.381	22.8	9.20
	360 eV [d]	PBEsol+D3	-45.5	21.861	27.5	10.79
		Expt.	-46.6 [e]	22.59 [f]	27.9 [p]	10.7 [p]
					25.2 [p]	12.3 [p]
α-Sn	$Fd\overline{3}m$ (# 227) [a]	PBE	0	36.799	36.3	4.88
	(23×23×23) [b]	PBEsol	0	35.049	41.9	4.85
	8 atoms [c]	PBE+D3	0	36.125	38.3	5.29
	150 eV [d]	PBEsol+D3	0	34.513	44.5	4.98

		Expt.	0	34.16 [f]	54 [q]	N/A
fcc Cu	$Fm\bar{3}m$ (# 225) [a]	PBE	0	12.027	137.0	4.94
	(34×34×34) [b]	PBEsol	0	11.372	163.0	4.93
	1 atom [c]	PBE+D3	0	11.369	159.3	4.87
	360 eV [d]	PBEsol+D3	0	10.870	181.9	4.97
		Expt.	0	11.81 [f]	133 [r]	5.30 [r]
					142 [s]	
bcc Li	$Im\bar{3}m$ (# 229) [a]	PBE	0	20.326	13.8	2.68
	(29×29×29) [b]	PBEsol	0	20.350	13.6	2.33
	2 atom [c]	PBE+D3	0	19.098	13.6	3.69
	360 eV [d]	PBEsol+D3	0	19.521	12.8	3.01
		Expt.	0	21.44 [f]	11.57 [t]	3.39±0.02 [t]
hcp Zn	$P6_3/mmc$ (# 194) [a]	PBE	0	15.491	58.7	5.01
	(35×35×15) [b]	PBEsol	0	14.394	75.5	5.21
	2 atoms [c]	PBE+D3	0	14.359	65.5	7.57
	360 eV [d]	PBEsol+D3	0	13.589	86.6	6.53
		Expt.	0	15.21 [f]	65±2 [u]	4.6±0.5 [u]
					73 [s]	

[a] Space group and its number in parentheses.

[b] k-points mesh used in the present first-principles calculations.

[c] Total atoms in unit cell used in the present first-principles calculations.

[d] Cut-off energy used in the present first-principles calculations.

[e] SGTE (SSUB) data at 298 K estimated based on experimental data.[79]

[f] Measured lattice parameters at room temperature (Å):[63] a = 5.708 for Li$_2$S; a = 3.795 and c = 16.342 for CuS; a =5.410 for ZnS; a = 5.4335 and c = 10.8429 for Cu$_2$ZnSnS$_4$ (CZTS); a = 11.143, b = 3.971, and c = 4.336 for α-SnS; a = 8.878, b = 3.751, and c = 14.050 for α-Sn$_2$S$_3$; a = 3.645 and c = 5.891 for α-SnS$_2$; a = 6.4892 for α-Sn; a = 3.614 for fcc Cu; a = 3.50 for bcc Li; a = 2.6647 and c = 4.9469 for hcp Zn.

[g] Based on c_{11}= 95.4±3.5 and c_{12} = 20.9±2.3 GPa via the measured acoustic phonons at 15 K.[80]

[h] Fitted results based on measured data at high pressures.[81]

[i] Fitted results based on diffraction data below 11 GPa,[82] note that other predictions of B_0' from first-principles are 4~5.[93]

[j] Fitted results based on measured data at high pressures.[83]

[k] Fitted results based on measured data at high pressures with constrained $B_0' = 4$.[84]

[l] Direct measurements of ΔH are not available for CZTS. Some first-principles results (kJ/mole-atom) are -42.1 by PBE,[29] -45.2 by PW91,[94] and -50.8 by PW91.[95] An indirect estimation based on sputtering rates measurement of Cu$_{1.9}$Zn$_{1.5}$Sn$_{0.8}$S$_4$ is -116±12 kJ/mole-atom.[85]

[m] Measurement is not available, this value is an estimated bulk modulus[96] based on an empirical relation for chalcopyrite compounds.[97]

[n] Fitted results based on measured data at high pressures.[86]

[o] Measurement is not available for Sn$_2$S$_3$, this value is an average for reference only based on bulk moduli of SnS and SnS$_2$.

[p] Fitted results based on measured data at high pressures with 25.2 GPa and 12.3 from the Vinet EOS and 27.9 GPa and 10.7 from the Birch-Murnaghan EOS.[87]

[q] Based on Raman scattering data at 77 K.[88]

[r] Fitted results based on measured data at high pressures.[89]

[s] Measured bulk moduli (GPa) at 0 K or 4.2 K.[60, 90]

[t] Fitted results based on measured data at high pressures.[91]

[u] Fitted results based on measured data at high pressures.[92]

Table 3

Calculated and experimental macroscopic static dielectric constants parallel to *a*-, *b*-, and *c*-axis of α-S.

Methods	// a-axis	// b-axis	// c-axis
PBEsol [a]	3.88	4.23	5.26
PBE+D3 [b]	3.93	4.30	5.28
PBEsol+D3 [b]	4.02	4.40	5.44
HSE06 [a]	3.47	3.77	4.53
Expt.[66]	3.65	3.85	4.66
Expt.[66]	3.59	3.83	4.62

[a] Calculated at equilibrium volume from PBEsol, see Table 1.

[b] Calculated at experimental volume, see Table 1.

Table 4

Calculated and experimental elastic constants c_{ij}'s and the corresponding polycrystalline aggregate properties of bulk modulus (B), shear modulus (G), Young's modulus (Y) and Poisson's ratio (ν) of α-S. Note that (i) Debye temperature Θ_0 (K) is estimated from Poisson's ratio, see equation (S3)[†]; (ii) the subscript "Hill" represents the Hill average based on the c_{ij} values,[72] and (iii) the unit for elastic properties is GPa.

Methods	c_{11}	c_{22}	c_{33}	c_{12}	c_{13}	c_{23}	c_{44}	c_{55}	c_{66}	B_{Hill}	G_{Hill}	Y_{Hill}	ν_{Hill}	Θ_0
PBEsol	9.4	9.8	13.2	1.4	-0.3	1.9	7.5	4.4	3.7	4.2	4.9	10.6	0.08	170
PBE+D3	12.9	11.2	17.7	2.1	2.0	6.6	7.4	4.4	3.5	6.8	4.9	11.9	0.21	173
PBEsol+D3	24.8	24.6	30.8	4.7	3.2	10.6	12.8	7.4	7.2	12.9	9.3	22.4	0.21	223
LDA	27.9	29.8	41.4	6.0	2.7	11.7	16.5	8.7	9.3	15.2	11.7	27.9	0.19	258
Expt.77[a]	19.2	17	23.2	4.6	5	11.3	10.9	4.3	5.8	11.0	6.3	15.9	0.26	196
Expt.293[a]	14.22	12.68	18.3	2.99	3.14	7.95	8.27	4.28	4.37	8.0	5.2	12.8	0.23	177
Expt.dyn[a]	19.8	17.2	23	5.5	6.1	14.3	9.3	3.2	5.6	12.1	5.3	13.8	0.31	180

[a] Adiabatic elastic constants measured at 77 K and 293 K,[65] and estimated based on the lattice dynamical calculations (dyn).[65]
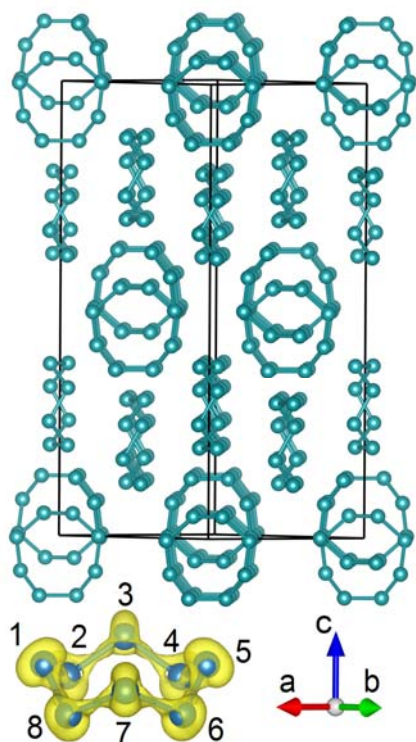
Figures and Figure Captions

Figure 1 Orthorhombic α-S (space group *Fddd*) composed of the crown-shape S_8 rings, which are roughly parallel or perpendicular to each other. One S_8 ring, consisting of atoms 1, 2, …, 8, and its differential charge density ($\Delta\rho/\text{Å}^3$, charge gain shown in yellow colors) predicted from PBEsol are also shown.
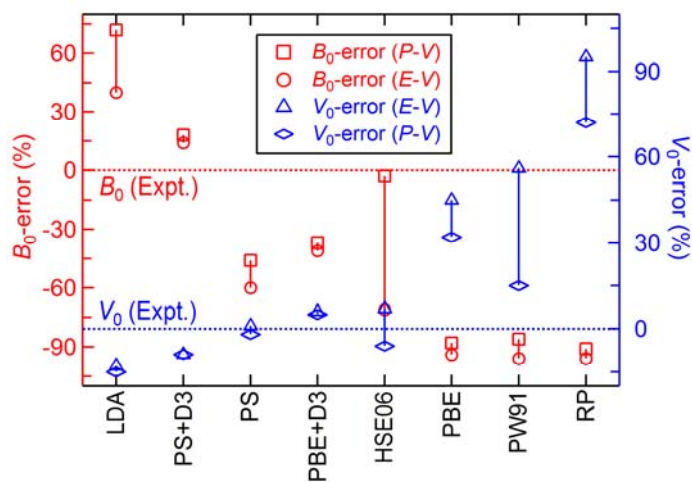
Figure 2 Calculated errors of bulk modulus (B_0 in red) and equilibrium volume (V_0 in blue) with respect to experimental data for α-S. Predictions are based on both the *P-V* EOS and the *E-V* EOS in terms of different X-C functionals. Note that (i) these data are also shown in Table 1 and (ii) the PS represents the PBEsol, and (iii) the calculated V_0 and B_0 at room temperature for two examples of α-S and Li_2S are given in Table S4[†].

(a)

(b)
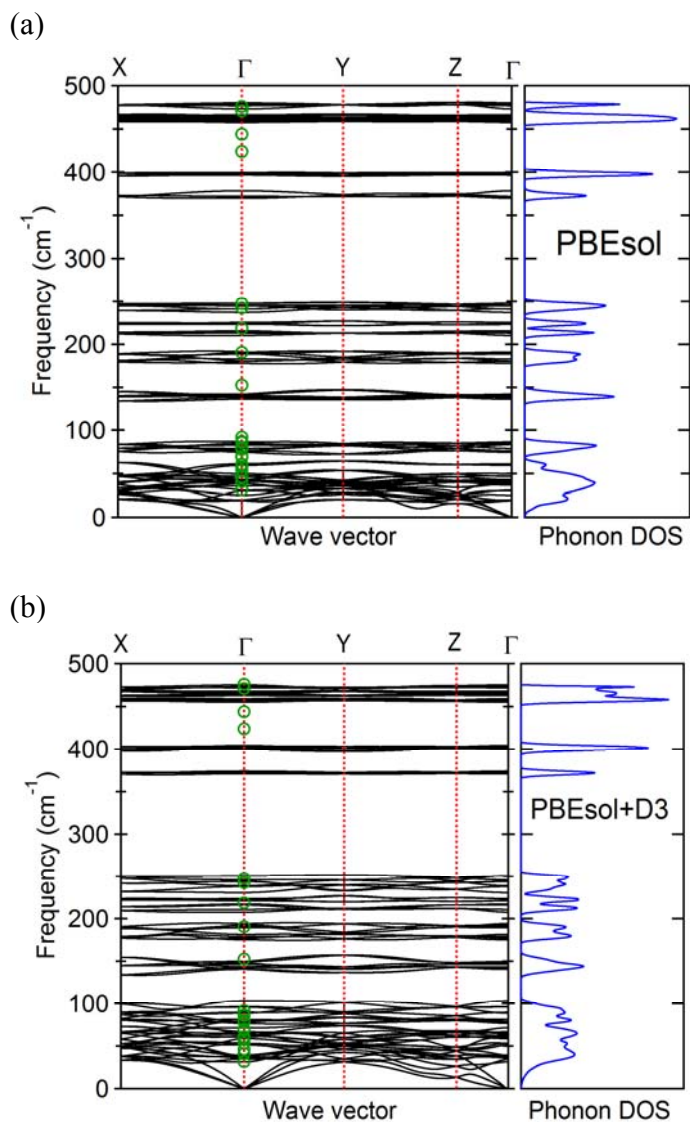
Figure 3 Calculated phonon dispersions and phonon density of state (DOS) of α-S at its theoretical equilibrium volume in terms of PBEsol (a) and PBEsol+D3 (b). Measured frequencies at Γ point by Raman and infrared spectra[66] are shown by green circles, and these dispersion curves have no obvious differences with and without the LO-TO splitting, see Table S3† for more details. Note that predicted results of α-S from LDA and PBE+D3 are shown in Figure S1.†
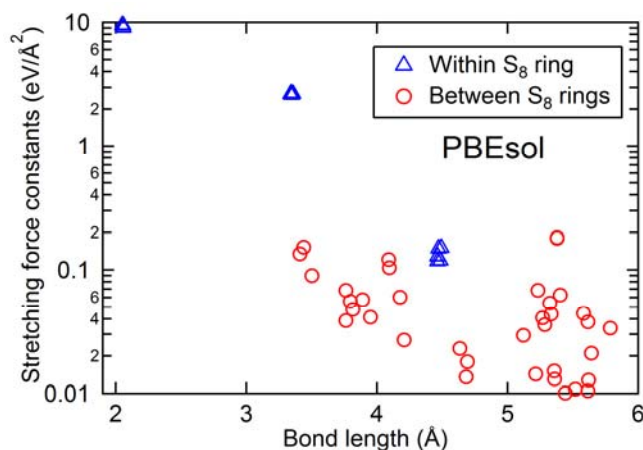
Figure 4 Key stretching force constants of α-S (from phonon calculations) with bond length less than 6 Å predicted from PBEsol. The ordinate is on a log scale. A large positive force constant suggests strong interaction, while the small values (< 0.01 eV/Å^2) are ignored in this plot. The stretching force constants around -0.34 eV/Å^2 are also ignored, which are for atomic pairs within the S_8 ring and possessing the longest bond lengths ($\sim$ 4.0-4.75 Å).
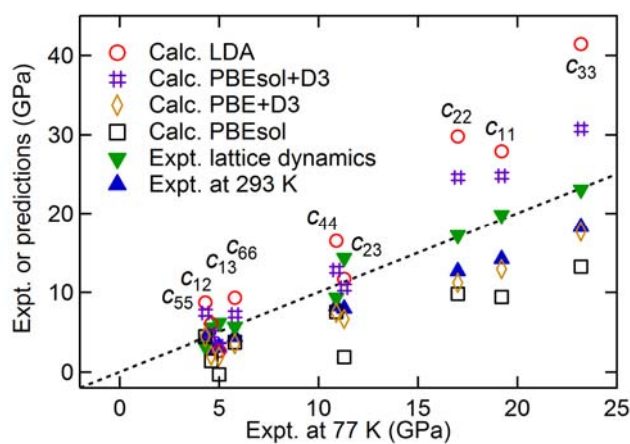

Figure 5 Measured elastic constants of α-S at 77 K[65] in comparison with experimental data at 293 K[65] and estimations from lattice dynamics data[65] as well as predictions by LDA, PBEsol+D3, PBE+D3 and PBEsol, see also Table 4.
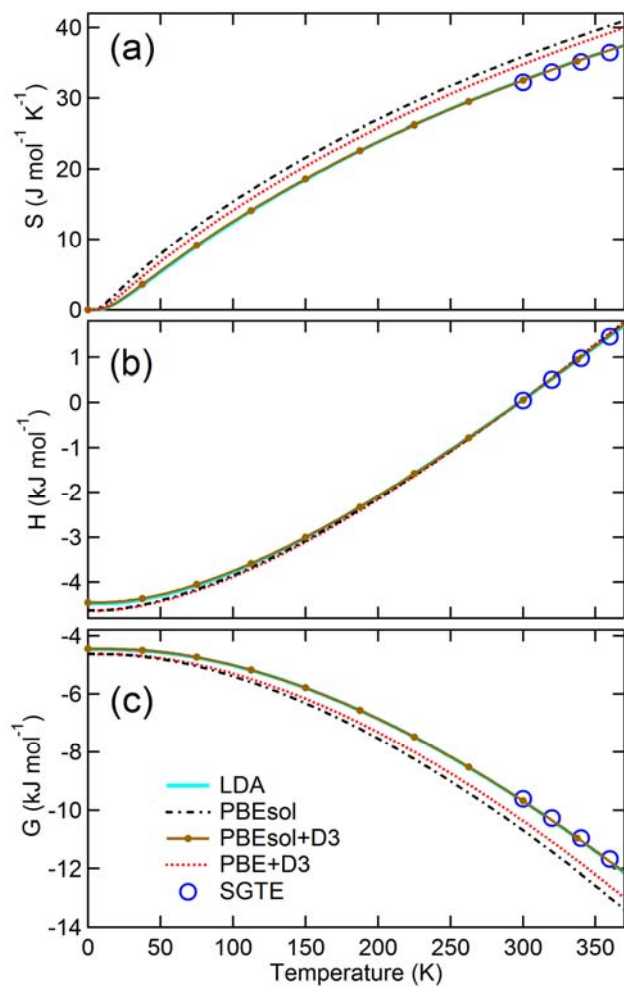
Figure 6 Entropy (S), enthalpy (H) and Gibbs (G) enegy of α-S predicted by LDA, PBEsol, PBEsol+D3, and PBE+D3. The circles are the SGTE data.[76]
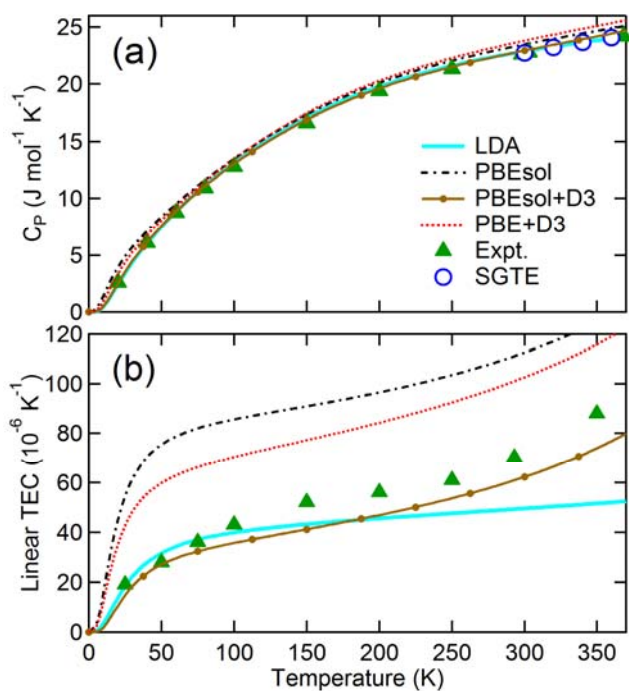
Figure 7 Heat capacity at constant pressure (C_P) and linear thermal expansion coefficient (TEC) of α-S predicted by LDA, PBEsol, PBEsol+D3, and PBE+D3, in comparison with the SGTE data[76] and measurements of the linear TEC[78] and C_P.[66]
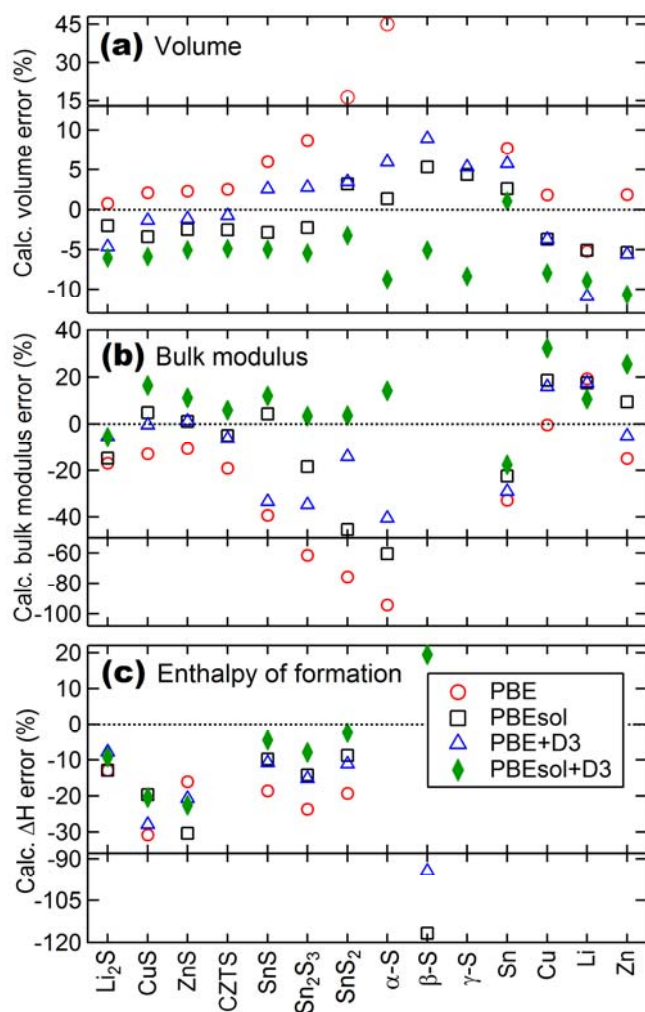
Figure 8 Calculated errors of equilibrium volume (a), bulk modulus (b) and enthalpy of formation ΔH (c) with respect to experimental data for S-containing energy materials and their constituent elements. Predictions are based on the *E-V* EOS in terms of different X-C functionals. See also Table 2 for details. Note that the calculated equilibrium volume (V_0) and bulk modulus (B_0) at room temperature for two examples of α-S and Li$_2$S are given in Table S4[†].